Received: 6 December 2020 | Revised: 12 February 2021 | Accepted: 14 February 2021

DOI: 10.1002/nbm.4500

RESEARCH ARTICLE

NMR IN BIOMEDICINE WILEY

An efficient $R_{1\rho}$ dispersion imaging method for human knee cartilage using constant magnetization prepared turbo-FLASH

Yuxi Pang[1] | Riann M. Palmieri-Smith[2,3] | Tristan Maerz[3]

[1]Department of Radiology, University of Michigan, Ann Arbor, Michigan

[2]School of Kinesiology, University of Michigan, Ann Arbor, Michigan

[3]Department of Orthopaedic Surgery, University of Michigan, Ann Arbor, Michigan

Correspondence
Yuxi Pang, PhD, Department of Radiology, University of Michigan, 1500 E. Medical Center Dr., Ann Arbor, MI 48109-5030, USA.
Email: yuxipang@umich.edu

Funding information
University of Michigan - Peking University Health Science Center (UM-PUHSC) Joint Institute: A Discovery Grant; National Institutes of Health, Grant/Award Number: 5-R01-HD-093626-02

This work aimed to develop an efficient $R_{1\rho}$ dispersion imaging method for clinical studies of human knee cartilage at 3 T. Eight constant magnetizations (M_{prep}) were prepared by tailoring both the duration and amplitude (ω_1) of a fully refocused spin-lock preparation pulse. The limited M_{prep} dynamic range was expanded by the measure, equivalent to that with $\omega_1 = \infty$, from the magic angle location in the deep femoral cartilage. The developed protocol with M_{prep} = 60% was demonstrated on one subject's bilateral and two subjects' unilateral asymptomatic knees. The repeatability of the proposed protocol was estimated by two repeated scans with a three-month gap for the last two subjects. The synthetic $R_{1\rho}$ and R_2 derived from $R_{1\rho}$ dispersions were compared with the published references using state-of-the-art $R_{1\rho}$ and R_2 mapping (MAPSS). The proposed protocol demonstrated good (<5%) repeatability quantified by the intra- and intersubject coefficients of variation in the femoral and tibial cartilage. The synthetic $R_{1\rho}$ (1/s) and the references were comparable in the femoral (23.0 ± 5.3 versus 24.1 ± 3.8, P = 0.67) and the tibial (29.1 ± 8.8 versus 27.1 ± 5.1, P = 0.62), but not the patellar (16.5 ± 4.9 versus 22.7 ± 1.6, P < 0.01) cartilage. The same trends were also observed for the current and the previous R_2. In conclusion, the developed $R_{1\rho}$ dispersion imaging scheme has been revealed to be not only efficient but also robust for clinical studies of human knee cartilage at 3 T.

KEYWORDS
fully refocused spin-lock preparation, human knee articular cartilage, magic angle effect, quantitative $R_{1\rho}$ dispersion imaging, tailored constant $R_{1\rho}$ weighting, turbo-FLASH

1 | INTRODUCTION

Water proton MR relaxation is not only an important factor governing an exquisite soft-tissue contrast in clinical MR imaging,[1] but it also becomes a powerful tool for studying in detail the structural and dynamic information about biological tissues.[2–4] One such parameter is the longitudinal relaxation ($T_{1\rho}$= $1/R_{1\rho}$) in a rotating frame, which has been demonstrated to provide unique insights into water-macromolecule interactions.[5–8] The observed relaxation rate $R_{1\rho}$ depends predominantly on a spin-lock (SL) amplitude ω_1; in other words, $R_{1\rho}$ varies with ω_1—a well known phenomenon referred to as $R_{1\rho}$ dispersion in the literature.[5,8] As early as the 1970s, $R_{1\rho}$ dispersion had been utilized for investigating pathophysiological changes in biological samples.[5] Two decades later, the first $R_{1\rho}$ imaging study on articular cartilage degeneration was reported,[9] and since then considerable efforts have been devoted to developing and standardizing $R_{1\rho}$ mapping methodology across primary MR system platforms in clinical settings.[8,10–13]

Abbreviations: CV, coefficient of variation; DZ, deep zone; FA, flip angle; FLASH, fast low angle shot; HR, hit rate; MAPSS, magnetization-prepared angle-modulated partitioned *k*-space spoiled gradient echo snapshots; M_{prep}, spin-lock prepared magnetization; PG, proteoglycan; REF, internal reference; ROI, region of interest; SD, standard deviation; SENSE, sensitivity encoding; SL, spin-lock; SZ, superficial zone; T_{SL}, spin-lock time; ω_1, spin-lock amplitude.

$R_{1\rho}$ could be viewed as a specific transverse relaxation rate (R_2) under the influence of an applied SL RF pulse, and it is particularly sensitive to low-frequency water molecular interactions.[5,7,14] $R_{1\rho}$ mapping of articular cartilage has been motivated by the diagnostic utility of a non-invasive and sensitive imaging method that can detect early cartilage degeneration in the absence of structural changes apparent on standard MRI.[11,15–17] $R_{1\rho}$ was first proposed as a promising MR biomarker for characterizing changes in proteoglycan (PG) content, but the specificity of its changes with PG alterations is not yet well understood.[8,15,18] The existing preclinical and clinical evidence suggests that $R_{1\rho}$ itself is not specifically sensitive to PG alterations, but rather $R_{1\rho}$ dispersion is predominantly susceptible to collagen changes, which are characterized by the residual dipolar interaction of ordered water molecules buried inside of collagen triple-helical microstructures.[7,8,19,20] These observations are in accordance with two previous studies from the early 2000s[21,22] as well as with some recent investigations relevant to the underlying $R_{1\rho}$ relaxation mechanisms in cartilage.[19,20,23]

Recently, a theoretical framework of $R_{1\rho}$ dispersion in cartilage has been outlined,[7] suggesting that an orientation-independent MR metric, named the order parameter, S,[24] can be derived for detecting early collagen degeneration in joint osteoarthritis. Traditionally, the $R_{1\rho}$ dispersion profile was obtained by collecting a series of $R_{1\rho}$ mappings by varying ω_1, with each $R_{1\rho}$ mapping in turn being created from another series of $R_{1\rho}$-weighted images with varying SL durations (T_{SL}).[7,8,25] As demonstrated schematically in Figure 1C, the standard $R_{1\rho}$ dispersion imaging (white dots) takes an unrealistically long acquisition time; thus, it is deemed to be impractical for clinical studies.

Apart from a lengthy acquisition time, it is also challenging to persistently obtain a reliable $R_{1\rho}$ under various ω_1 conditions using a magnetization-prepared spoiled turbo-FLASH (fast low angle shot) sequence.[17,26,27] The potential $R_{1\rho}$ quantification errors could be introduced during SL preparation and/or during imaging readout. It has been well documented that the prepared SL magnetization (M_{prep}) is highly susceptible to B_0 and B_1 non-uniform field artifacts.[28–32] Although many advanced SL schemes, including those using adiabatic pulses, have been developed in the past, none of these methods was specifically designed or optimized for $R_{1\rho}$ dispersion imaging using a broad range of ω_1.

The prepared M_{prep}, on the other hand, could be further compounded by an adverse T_1 relaxation effect, stemming from the prepared transient signal evolution towards steady state during imaging readout.[17,27] To mitigate this detrimental effect, advanced pulse sequences including RF phase cycling and tailored excitation flip angles (FAs) have been proposed[17,33]; however, these advanced techniques are not suitable for clinical $R_{1\rho}$ dispersion imaging because of a twofold increase in acquisition time as well as the complexity of tailoring FA schemes.

To further explore $R_{1\rho}$ dispersion of articular cartilage in clinical studies, there exists an unmet need to develop a reliable acquisition protocol without substantially increasing the imaging time. Hence, the aim of this work was to develop a practical $R_{1\rho}$ dispersion imaging method for clinical studies of the human knee cartilage. The proposed protocol was evaluated on four human asymptomatic knees from three adult volunteers at 3 T, and the results were compared with those measured with the state-of-the-art $R_{1\rho}$ mapping sequences (magnetization-prepared angle-modulated partitioned k-space spoiled gradient echo snapshots; MAPSS) in the literature.[17]

2 | METHODS

2.1 | Constant $R_{1\rho}$ weighting using tailored T_{SL} and ω_1

An image voxel signal $S(T_{SL}, \omega_1)$ from $R_{1\rho}$-weighted image of cartilage[7] can be expressed using the equations 1-2

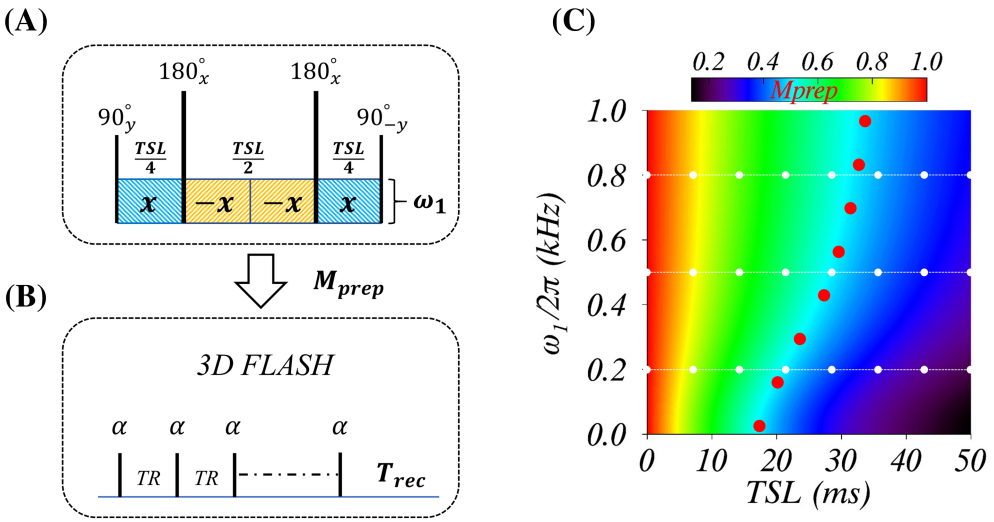

FIGURE 1 Schematic diagram of the proposed $R_{1\rho}$ dispersion imaging sequence including a fully refocused SL preparation (A) for a spoiled turbo-FLASH readout (B), and a prepared constant (red dots) SL magnetization M_{prep} (C)

$$S(T_{SL},\omega_1) = S_0 \exp\left(-R_{1\rho}T_{SL}\right) \quad (1)$$

$$R_{1\rho} = R_2^i + \frac{R_2^{ex}}{1+4\omega_1^2\tau_{ex}^2} + \frac{R_2^a(\theta)}{1+4\omega_1^2\tau_b^2} \quad (2)$$

where S_0, R_2^i, R_2^a and R_2^{ex} denote respectively the initial signal, isotropic and anisotropic dipolar relaxation rates, and chemical-exchange-induced relaxation rate. Here, the chemical exchange time and the anisotropic dipolar interaction correlation time are represented by τ_{ex} and τ_b, respectively. Note that R_2^{ex} contributes only a few percent to $R_{1\rho}$ in cartilage at 3 T, and thus it can be safely disregarded from Equation 2.[7,8] Accordingly, R_2^{ex} was set to zero in this work unless stated otherwise.

$R_2^a(\theta)$ is normally written as $R_2^a 3\cos^2\theta - 1^2/4$, with θ the angle between the collagen fiber primary direction in the deep femoral cartilage and B_0[7,34]; consequently, $R_{1\rho}$ will become R_2^i when $\theta = 54.7^\circ$, the so-called magic angle. On the other hand, the same result can also be obtained when $\omega_1 = \infty$. This fact has been exploited herein to increase the limited dynamic range in the prepared M_{prep}, defined as $\exp(-R_{1\rho}T_{SL})$. More specifically, the signal derived from $\theta = 54.7^\circ$ in the deep femoral cartilage was treated as that with $\omega_1 = \infty$. This extra information, ie $S_0 \exp\left(-R_2^i T_{SL}\right)$, has been referred to as an internal reference (REF) in the literature.[23]

To our knowledge, only two quantitative $R_{1\rho}$ dispersion investigations on the human knee cartilage in vivo at 3 T have been reported in the past.[7,25] The so-called inflection point (ω_{ip}) on the $R_{1\rho}$ dispersion curve is determined by setting the second derivative of Equation 2 to zero, leading to the relationship $1/\tau_b = 2\sqrt{3}\omega_{ip}$. An average τ_b of 262 ± 58 μs could be thus obtained based on the reported ω_{ip} values,[25] consistent with the previous estimation.[7] Hence, a τ_b of 300 μs was chosen for numerical simulations in this work. Additionally, R_2^i and R_2^a were estimated to be 20 (1/s) based on the measured $R_{1\rho}$ dispersion profiles in Figure 3A from the original paper.[25] Given all these assumed values, a specific M_{prep} can be calculated by a judicious combination of T_{SL} and ω_1 in Equations 1 and 2 (see Figure 1C). One constant M_{prep} of 60% was prepared and tabulated in Table 1, containing eight pairs of T_{SL} and $\omega_1/2\pi$, with the former ranging from 13 to 24 ms and the latter from 0 to 1 kHz.

2.2 | A practical $R_{1\rho}$ dispersion imaging protocol

To ensure a reliable prepared M_{prep} that can be subsequently measured as much as possible during imaging readout, an improved SL preparation and an optimal FA (see below) in a FLASH sequence were implemented for the proposed $R_{1\rho}$ dispersion imaging method. A pair of refocusing RF pulses (180°) was inserted in the middle of two pairs of antiphase rotary-echo pulses as sketched in Figure 1A, leading to fully refocusing the chemical shift ($\Delta\omega_0$) artifacts from non-uniform B_0 even when the FA of the refocusing pulse was not exactly equal to 180° because of B_1 inhomogeneity.[32,35]

$R_{1\rho}$ dispersion imaging was performed on an Ingenia 3 T MR system (Philips Healthcare, Best, The Netherlands) in the sagittal plane, using a 16-channel T/R knee coil that was capable of generating an SL amplitude as high as 1150 Hz, ie a maximum $B_1 \sim 27$ μT. Each $R_{1\rho}$-weighted image was acquired using a pair of $T_{SL}$and ω_1 as listed in Table 1. The key acquisition parameters were as follows: SL 90°/180° RF durations = 0.25/0.5 ms; field of view = 130 × 130 × 96 mm^3; acquired voxel size = 0.6 × 0.6 × 3.0 mm^3; number of slices = 32; compressed sensitivity encoding (SENSE)[36] factor = 2.5; fat suppression = "binomial (1-2-1) pulse triplet for α pulse in FLASH readout". The other relevant FLASH parameters were as follows: number of profiles N = 64; TR/TE = 6.8/3.5 ms; acquisition bandwidth = 573 Hz/pixel; shot interval = 2 s; number of shots (or segments) = 34. An optimal FA of 13° was derived analytically[1,37] given M_{prep} = 60%, T_1 = 1240 ms,[17] TR = 6.8 ms, and N = 64. The phase-encoding order was segmented elliptical centric with outward spiral. One $R_{1\rho}$-weighted 3D image dataset took 1.15 min, leading to 9.2 min for $R_{1\rho}$ dispersion imaging using a constant M_{prep}.

Three consenting volunteers, who were recruited for an IRB-approved clinical study on joint cartilage degeneration, participated in this work. The protocol with M_{prep} = 60% was used for the first subject, with bilateral (asymptomatic) knees scanned, and for the second and the third subjects with a unilateral (asymptomatic) knee imaged. To investigate the repeatability of the proposed imaging method, the last two subjects were rescanned after three months.

For comparative purposes, some key acquisition parameters from our previously used standard $R_{1\rho}$ dispersion imaging were provided as follows[7]: ie five $\omega_1/2\pi$ settings ranging from 0.125 to 1.0 kHz; five T_{SL} values from 1 to 40 ms per $\omega_1/2\pi$ setting; SL method = "rotary-echo".[29] Compressed SENSE[36] factor = 3.0; TR/TE = 8.5/4.3 ms; acquisition bandwidth = 382 Hz/pixel; FA = 10°; acquired voxel size = 0.4 × 0.4 × 3.0 mm^3.

TABLE 1 A constant prepared SL magnetization (M_{prep} = 60%) with eight pairs of SL RF durations (T_{SL}) and amplitudes ($\omega_1/2\pi$). These tailored settings were based on $R_2^i = R_2^a$ = 20 (1/s), τ_b = 300 μs and R_2^{ex} = 0

Scan index	1	2	3	4	5	6	7	8
T_{SL} (ms)	13	14	16	19	21	22	23	24
$\omega_1/2\pi$ (Hz)	0	120	220	360	500	600	740	1000

Each $R_{1\rho}$ mapping took 8.75 min, and the total scan time for a complete $R_{1\rho}$ dispersion imaging was 43.75 min. The success fitting rates (see below) for $R_{1\rho}$ dispersion were respectively 35%, 49% and 36% for the femoral, tibial and patellar cartilage. The fitted model parameters (R_2^i, R_2^a, τ_b and S) can be found in Table 3 from the published paper,[7] and were compared with those derived from the current study using the developed $R_{1\rho}$ dispersion imaging protocol (M_{prep} = 60%).

2.3 | Nonlinear least-squares curve fitting

Before quantifying $R_{1\rho}$ dispersion, $R_{1\rho}$-weighted 3D images, including an intra- and an inter-series acquired from each subject's unilateral knee, were co-registered using the free software *elastix*[38] following an established protocol.[23] Then, the femoral, tibial and patellar cartilage was manually outlined using the free software ITK-SNAP,[39] followed by an angular-radial segmentation as previously demonstrated.[23] Note that, for the tibial and patellar cartilage, the angular segmentations were evenly partitioned into five regions of interest (ROIs) horizontally and vertically. Nonetheless, the radial segmentations were the same for all three knee cartilage compartments. The data analysis was performed on the segmented ROIs in the deep (DZ) and superficial (SZ) zones of the cartilage.

Equations 1 and 2 were fitted to average $R_{1\rho}$-weighted voxel values derived from segmented ROIs. The nonlinear least-squares curve fitting was performed using a publicly available IDL script based on the Levenberg-Marquardt algorithm (http://purl.com/net/mpfit).[40] It should be stressed that there were *two independent* variables, ie T_{SL} and ω_1, in this unusual data modeling, where four model parameters (ie S_0, R_2^i, R_2^a, τ_b) needed to be optimized. An unweighted fitting was employed in this study, where the uncertainties for each measurable were uniformly set to one. As a result, the output formal 1-sigma fitting errors had to be scaled so that the reduced chi-square χ^2 values were approximately equal to one.[40]

The fitted model parameters were constrained during χ^2 optimizations, ie S_0=[100, 1000]; R_2^i = [1, 20] (1/s); R_2^a = [0.5, 100] (1/s) and τ_b= [1, 1000] (μs), with initial values set to 500, 10, 20 and 250, respectively. Given the fitted R_2^a and τ_b, an order parameter S (Reference[7]) was calculated as $\sqrt{(2R_2^a)/\left(3d^2\tau_b\right)}$, with d denoting a constant of 1.028×10^5 (1/s). The uncertainty in S was also derived from the uncertainties of R_2^a and τ_b following the basic error propagation rules.[41] In highly ordered biological tissues, S characterizes an intrinsic property of bound water molecular reorientation anisotropy.[24]

An REF was determined as described before[23] for each of eight $R_{1\rho}$-weighted 3D image datasets, and included in the curve fitting to improve the accuracy of the fits due to an enhanced dynamic range of the measured data. Specifically, these REF signals were considered as those measured using the tailored T_{SL}values (ranging from 13 to 24 ms) and $\omega_1/2\pi$ = 10 kHz (rather than infinity). As a result, there were 16 measurable data in total for fitting the $R_{1\rho}$ dispersion profile of each of the segmented ROIs.

The goodness of fit was loosely defined by R^2, showing how much the observed $R_{1\rho}$ dispersion could be explained by the fitted model.[42] If fitted parameters were within the boundary values and their relative uncertainties did not exceed 100%, the fit was considered successful; otherwise, it was excluded from further analysis. A hit rate (HR%) was defined as the percent of successful fits from all the segmented ROIs within each cartilage compartment.

2.4 | Evaluations of $R_{1\rho}$ dispersion quantification

The prepared and the observed M_{prep} were evaluated for potential discrepancies. The proposed imaging protocol was designed with an assumption of $R_2^i = R_2^a$ = 20 (1/s), τ_b = 300 μs for a constant M_{prep} = 60%. The average fitted values for each of these model parameters over multiple (n = 6) measurements were calculated. Then, the measured M_{prep} dynamic ranges in the DZ and the SZ were determined using eight pairs of T_{SL} and $\omega_1/2\pi$, and compared with the prepared constant M_{prep}.

The duplicated $R_{1\rho}$ dispersion measurements, with a three-month gap on the second and the third subjects, were used to estimate the repeatability of the proposed imaging protocol. This basic statistical assessment, including an intra-subject and an inter-subject repeatability (see below), was performed only in the DZ on the fitted model parameters.

The state-of-the-art $R_{1\rho}$ mapping sequence MAPSS can provide an accurate $R_{1\rho}$ at the cost of doubling scan time.[17] A reference value of $T_{1\rho}$ ($\omega_1/2\pi$ = 500 Hz) at 3 T for each of six standardized segmented compartments in healthy knees (n = 7) was documented in Table 2 from the original paper.[43] These $T_{1\rho}$ values were converted into their reciprocals and then an average $R_{1\rho}$ of 24.1 ± 3.8 (1/s) was found for the femoral including trochlea, 27.1 ± 5.1/s for the tibial and 22.7 ± 1.6 (1/s) for the patellar cartilage.

For comparative purposes, a synthetic $R_{1\rho}$ was calculated using Equation 2 with $\omega_1/2\pi$ = 500 Hz and average fitted parameters in Table 2 from the current study. To estimate the precision of the synthetic $R_{1\rho}$, Monte Carlo simulations were performed for 1000 runs, each with average fitted parameters (R_2^i, R_2^a and τ_b) contaminated with Gaussian noise.[44] This normally distributed noise was characterized by zero mean and unit variance, corresponding to the propagated errors from the DZ and SZ. The means and the standard deviations (SDs) of 1000 simulated synthetic $R_{1\rho}$ values in different cartilage compartments were compared with the reported references. Following the same procedures, the fitted R_2, ie $R_2^i + R_2^a$, was also compared with the previously reported R_2 at 3 T that were measured using the MAPSS sequence in the same publication.[43]

TABLE 2 Average success fitting rates (HR%) and average fitted model parameters over six $R_{1\rho}$ dispersion measurements (M_{prep} = 60%) on three subjects in the DZ and the SZ within the femoral, tibial and patellar cartilage compartments

	DZ			SZ		
Fits	**Femoral**	**Tibial**	**Patellar**	**Femoral**	**Tibial**	**Patellar**
HR (%)	71.7 ± 12.3	87.2 ± 8.9	58.6 ± 13.5	66.2 ± 10.4	90.1 ± 9.4	21.1 ± 13.6
R_2^i (1/s)	10.8 ± 2.5	10.4 ± 2.8	10.7 ± 2.4	10.9 ± 2.4	10.8 ± 2.7	10.6 ± 2.3
R_2^a (1/s)	22.0 ± 3.1	39.1 ± 8.9	17.3 ± 5.2	15.6 ± 2.1	17.0 ± 2.9	8.3 ± 1.4
τ_b (μs)	109.7 ± 22.0	92.8 ± 17.3	115.8 ± 23.3	138.7 ± 48.3	138.1 ± 57.4	282.2 ± 74.2
S (10^{-3})	3.70 ± 0.59	5.11 ± 0.83	3.36 ± 0.68	2.91 ± 0.62	3.04 ± 0.72	1.45 ± 0.24

2.5 | Statistical analysis

The coefficient of variation (CV) was used to characterize an intra-subject repeatability of the measureable, calculated for subject i (i = 2,3) as $CV_i = SD_i/M_i$, where the SD_i and M_i denote the SD and the mean of the measureable from two repeated scans. On the other hand, the root mean square of CVs of individual subject, ie $CV_{rms} = \sqrt{\sum_{i=1}^{N} CV_i^2/N}$, with $N = 2$, was used to estimate an inter-subject repeatability.[45] Moreover, the stability of the observed M_{prep} was also quantified with CV, and an unpaired t-test was used to assess the differences between two relaxation parameters, with significant difference indicated by $P < 0.05$. All image and data analysis was performed using customized software developed in IDL 8.5 (Harris Geospatial Solutions, Broomfield, CO). All measurements are shown as mean ± SD unless stated otherwise.

3 | RESULTS

3.1 | An optimized $R_{1\rho}$ dispersion imaging sequence

The proposed $R_{1\rho}$ dispersion imaging sequence is shown schematically in Figure 1, with a fully refocused SL preparation scheme (A) implemented for a spoiled turbo-FLASH sequence (B). As previously demonstrated, by the numerical simulations and experimental studies at 3 T on a phantom and the human knee cartilage in vivo, the proposed SL scheme was less prone to B_0 and B_1 non-uniform field artifacts, particularly at the lower $\omega_1/2\pi$, when compared with the reported SL methods.[35] The prepared constant (red dots) M_{prep} is highlighted in the 2D M_{prep} map (C), with respect to the previously used varied (white dots) M_{prep} scheme.

3.2 | Quantitative $R_{1\rho}$ dispersion imaging

The measured (blue filled circles) and modeled (red and green solid lines) representative $R_{1\rho}$ dispersion profiles are demonstrated in Figure 2B and 2C. The measured data were obtained, as shown in Figure 2A, from a segmented ROI in the tibial deep cartilage (white arrow) and an REF location in the femoral deep cartilage (yellow arrow) of the first subject's left knee. The REF data could be easily recognized as the higher signals in Figure 2B and fitted by a straight (green) line because there was hardly any $R_{1\rho}$ dispersion around the magic angle locations. These REF data were absent from Figure 2C because they were out of the display range ($\omega_1/2\pi$=10 kHz).

The fitting success or HR% using the constant M_{prep} (60%) were much higher than those with the varied M_{prep}[7]; specifically, they were respectively 72% versus 35% (femoral), 87% versus 49% (tibial) and 59% versus 36% (patellar). Figure 3 presents an example of $R_{1\rho}$ dispersion quantification from the third subject's knee. An anatomical T1ρW sagittal image slice is shown (Figure 3A) with segmented ROIs superimposed. The ROI-based parametric color maps, R_2^i (Figure 3B), R_2^a (Figure 3C), τ_b (Figure 3D), S (Figure 3E) and R^2 (Figure 3F), were overlaid on the T1ρW image.

Around the trochlear cartilage, as indicated by a white arrow in Figure 3F, the decreased R^2 values revealed less reliable $R_{1\rho}$ dispersion quantification, probably resulting from a vanishing residual dipolar interaction near the magic angle orientation. It was challenging to manually segment the DZ precisely near the calcified cartilage[46]; hence, it was no surprising to observe some abrupt R_2^a changes as shown in the deep femoral cartilage, as shown in Figure 3C. However, an unusual high R_2^a in the deep tibial cartilage, as indicated by yellow arrows in Figure 3A and 3C, might not be well accounted for by an inaccurate segmentation. Both T2W (not shown) and T1ρW images showed relatively low signals at this particular tibial cartilage location, suggesting that the corresponding R_2^a relaxation was enhanced, as the R_2^i relaxation (Figure 3B) was relatively uniform across the tibial cartilage.

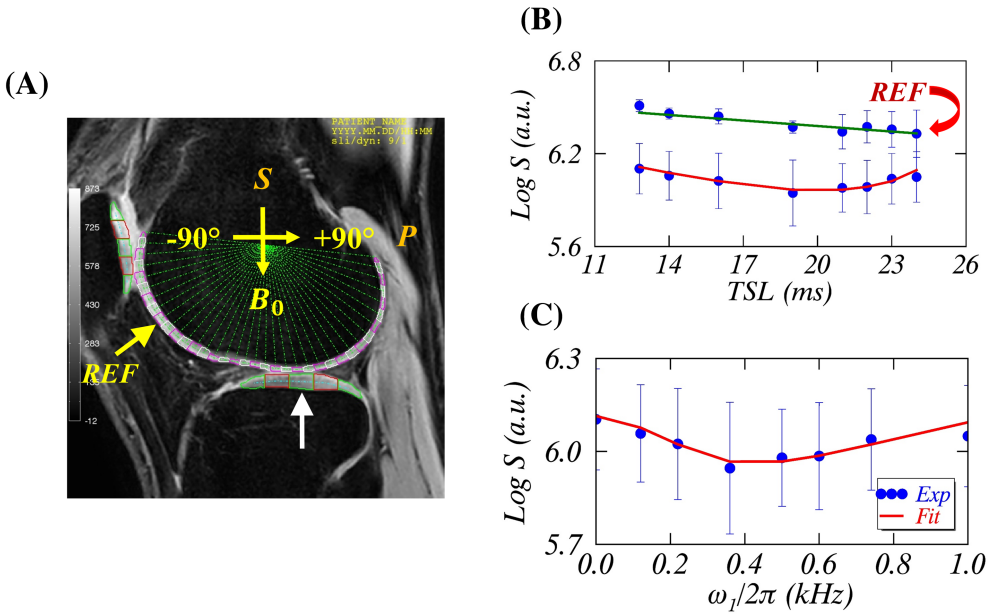

FIGURE 2 A, $R_{1\rho}$-weighted signals were measured from one segmented ROI in the deep tibial cartilage (white arrow), and the REF data were taken from the deep femoral cartilage (yellow arrow). B, C, Measured (blue filled circles) and fitted (red and green solid lines) exemplary $R_{1\rho}$ dispersion profile versus T_{SL} (B) and $\omega_1/2\pi$ (C)

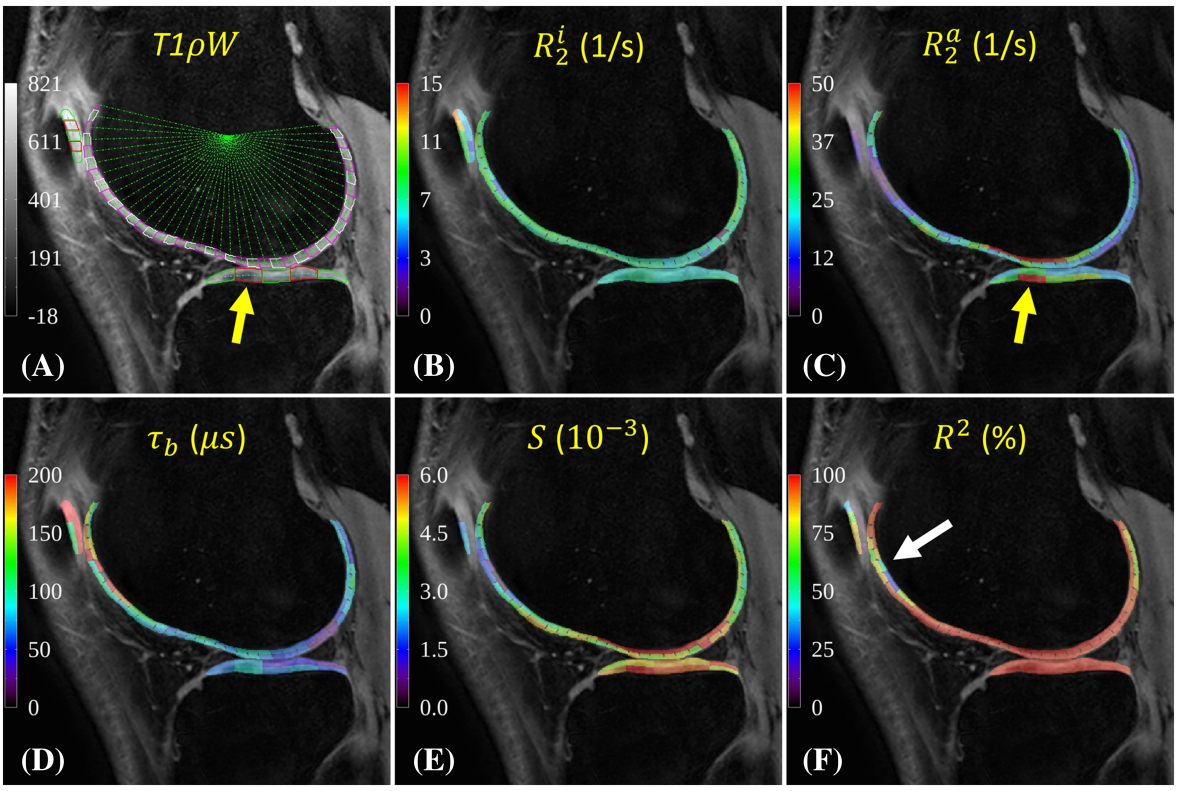

FIGURE 3 T1ρW sagittal image (A) with representative ROI-based parametric color maps of R_2^i (B), R_2^a (C), τ_b (D), S (E) and R^2 (F) derived from $R_{1\rho}$ dispersion imaging of the third subject's knee superimposed

3.3 | Developed and previous $R_{1\rho}$ dispersion imaging

Figure 4 compares the average fitted R_2^i (Figure 4A), R_2^a (Figure 4B), τ_b (Figure 4C) and S (Figure 4D) over six measurements in the DZ (red) and the SZ (green) using the developed $R_{1\rho}$ dispersion imaging protocol on three subjects, with those previously reported in the DZ* (blue) using the standard method on one subject,[7] in the femoral, tibial and patellar cartilage compartments.

The fitted values with the proposed protocol are also tabulated in Table 2, showing that the fits in the DZ were comparable to (ie R_2^i), smaller than (ie τ_b) and larger (ie R_2^a and S) than those in the SZ. When compared with the fits (red) from this work, the previously reported (blue) R_2^a (1/s) was significantly reduced in the femoral (11.3 ± 4.9 versus 22.0 ± 3.1, $P = 0.01$) and tibial (8.7 ± 4.1 versus 39.1 ± 8.9, $P < 0.01$) cartilage while the R_2^i (1/s) was not significantly ($P > 0.33$) different across all three cartilage compartments. On average, the previously reported τ_b and S values were respectively about twice and half those from the current study.

3.4 | Measured dynamic range of M_{prep}

Given the fitted R_2^i, R_2^a and τ_b in Table 2, the measured M_{prep} was calculated using eight combinations of T_{SL} and $\omega_1/2\pi$ for $M_{prep} = 60\%$ (Table 1), and plotted for the SZ (Figure 5A) and the DZ (Figure 5B) in the femoral (red), tibial (green) and patellar (blue) cartilage. Although some observed M_{prep} profiles considerably deviated from the initially designed M_{prep} (dashed lines), the variations of these measured M_{prep} were relatively small, eg with a CV of 8.3% in the deep tibial cartilage and of 1.3% in the superficial patellar cartilage.

3.5 | Precision and accuracy assessments

The values of CV and CV_{rms} for the fitted parameters (R_2^i, R_2^a, τ_b, S) were calculated. For Subject 2, the proposed $R_{1\rho}$ dispersion imaging protocol had provided a relatively precise measurement as indicated by an average intra-subject repeatability of CV_2=4.2 ± 2.1% for all fitted parameters over the whole cartilage. This observation was generally in line with an average inter-subject repeatability of CV_{rms}=4.6 ± 2.5% as shown in

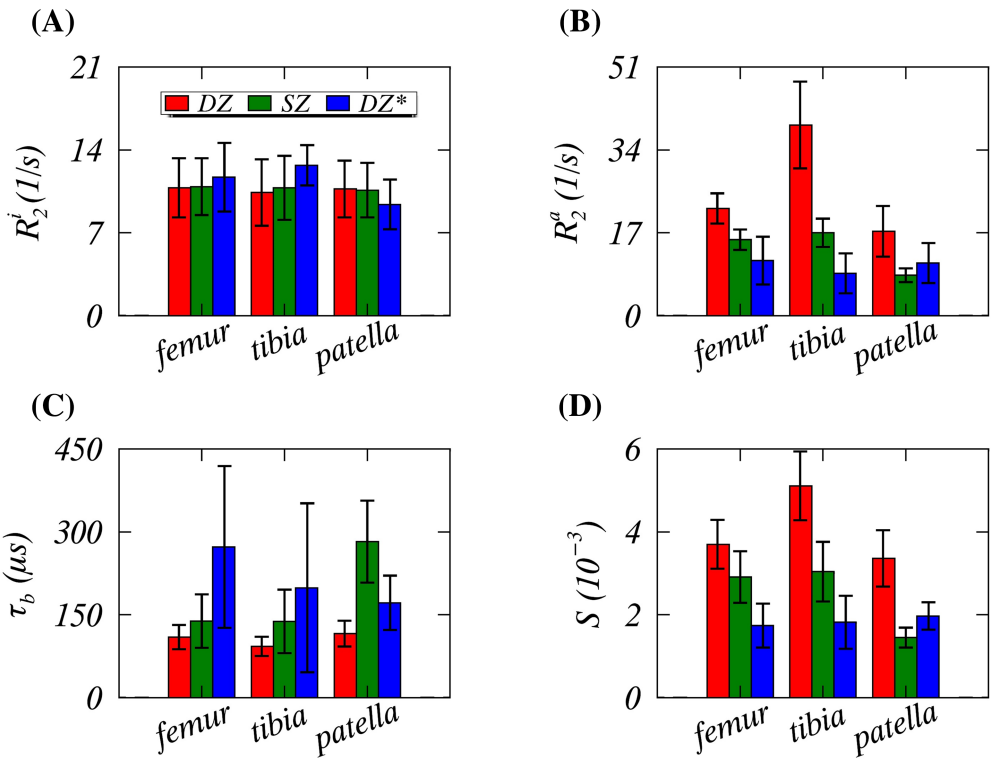

FIGURE 4 Averaged over six measurements from three subjects, the fitted parameters of R_2^i (A), R_2^a (B), τ_b (C) and S (D) compared in the DZ and the SZ of all three cartilage compartments. Also included are the related values in the deep zone (DZ*) derived from the previous standard $R_{1\rho}$ dispersion imaging

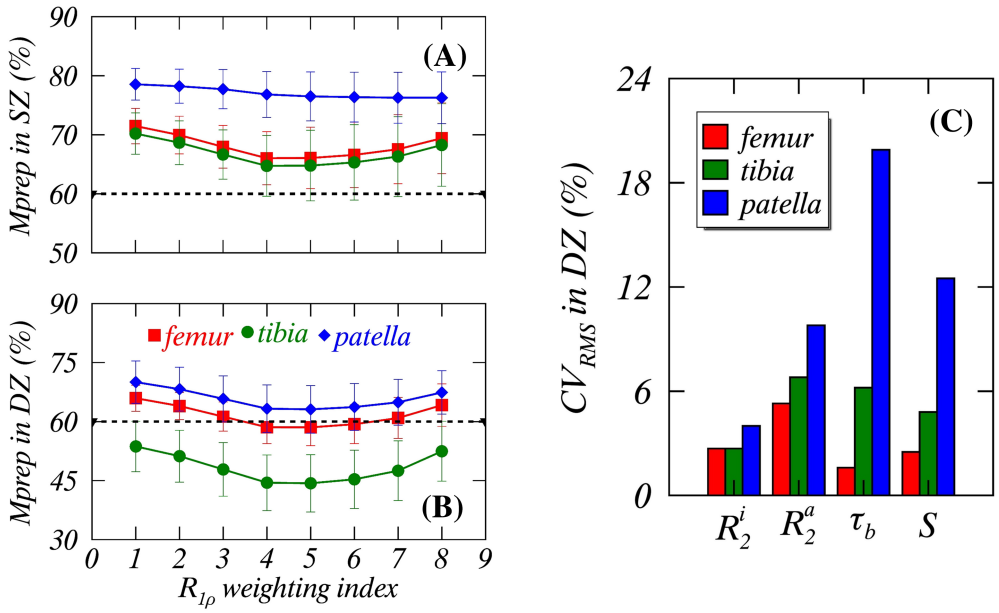

FIGURE 5 A, B, Measured average M_{prep} in the SZ (A) and the DZ (B) of the femoral, tibial and patellar cartilage compartments. The tailored M_{prep} is indicated by a horizontal dashed line. C, Inter-subject repeatability measures were compared for the fitted parameters (R_2^i, R_2^a, τ_b, S) in the deep femoral, tibial and patellar cartilage compartments

Figure 5C, when excluding those τ_b and S values in the patellar cartilage. It was unclear why CV_3 (from Subject 3) of the fitted parameters for the repeated scans were markedly diversified only in the patellar cartilage.

The differences between the synthetic $R_{1\rho}$ (1/s) (gold) and the references[43] from MAPSS (blue), as revealed in Figure 6A, were not statistically significant in the femoral (23.0 ± 5.3 versus 24.1 ± 3.8, $P = 0.67$) or tibial (29.1 ± 8.8 versus 27.1 ± 5.1, $P = 0.62$) cartilage, but this was not the case in the patellar (16.5 ± 4.9 versus 22.7 ± 1.6, $P = 0.01$) cartilage. Meanwhile, the synthetic $R_{1\rho}$ appeared to be less precise (ie with larger SDs) than that reported. The same trend, as shown in Figure 6B, was also observed when comparing the fitted R_2 (1/s) (gold) with the references[43] (blue), in the femoral (29.7 ± 5.1 versus 32.4 ± 4.9, $P = 0.34$), tibial (38.7 ± 10.1 versus 36.4 ± 7.4, $P = 0.66$) and patellar (23.5 ± 6.3 versus 32.5 ± 2.2, $P < 0.01$) cartilage.

4 | DISCUSSION

4.1 | General comments

An efficient acquisition method for $R_{1\rho}$ dispersion imaging of the human knee cartilage at 3 T has been developed in this work. The basic idea is to prepare the constant $R_{1\rho}$ weighting by simultaneously tailoring T_{SL} and ω_1 in a spoiled turbo-FLASH sequence. This unique method not only markedly reduces the total acquisition time but also alleviates the potential T_1 relaxation artifacts during FLASH imaging readout in the standard $R_{1\rho}$ mapping. The measurement results from repeated scans and from comparisons with the literature suggest that the proposed imaging method is a promising tool to further explore $R_{1\rho}$ dispersion in the human knee cartilage in clinical settings.

4.2 | Improved acquisition efficiency on $R_{1\rho}$ dispersion imaging

The primary advantage of the proposed method relies on its acquisition efficiency, making it feasible to employ in clinical studies. Traditionally, it has taken an unrealistically long scan time to collect multiple series of $R_{1\rho}$-weighted images with different ω_1. For instance, the first such study of in vivo human knee cartilage utilized 12 different ω_1, with each ω_1 setting for $R_{1\rho}$ mapping lasting more than 5 min using five different T_{SL} values, resulting in a total scan time of more than 1 h.[25] Similarly, our previous standard $R_{1\rho}$ dispersion imaging protocol took about 45 min using five ω_1, with each ω_1 for five T_{SL} settings.[7]

By contrast, the proposed $R_{1\rho}$ dispersion imaging protocol took only 9.2 min for eight constant $R_{1\rho}$-weighted images, and this practical acquisition time could be even shortened further by reducing the number of acquired $R_{1\rho}$ weightings. There are only four model parameters (ie S_0, R_2^i, R_2^a and τ_b, with $R_2^{ex} = 0$), as shown in Equations 1 and 2, and thus two acquisitions would suffice to determine these parameters given two extra

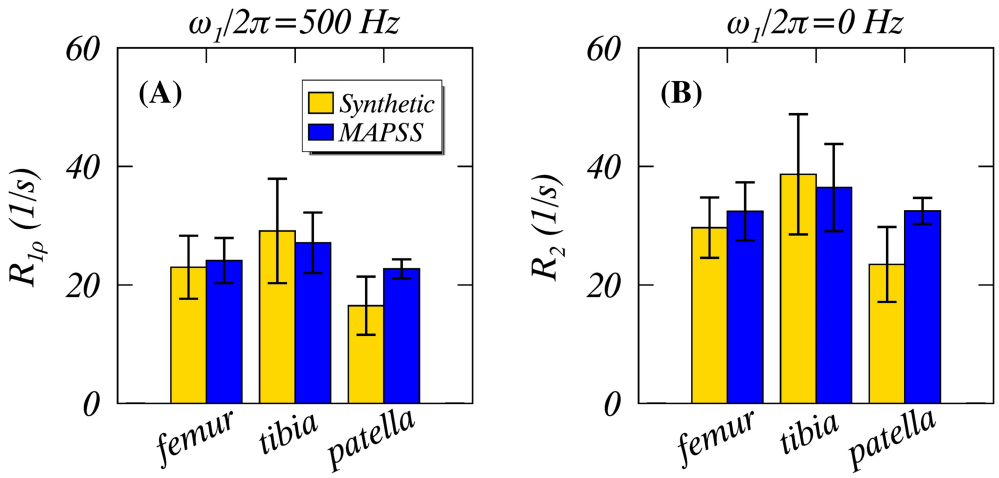

FIGURE 6 Average synthetic $R_{1\rho}$ (A) and R_2 (B), compared with the references measured using MAPSS sequences in all three cartilage compartments. The presented $R_{1\rho}$ and R_2 data with MAPSS were extracted from Reference 43

REFs. In fact, this concept has been exploited in our previous work to derive an anisotropic R_2^a from a single T_2-weighed image.[23] Nonetheless, it would be unwise to characterize $R_{1\rho}$ dispersion using only two acquisitions as it would to quantify $R_{1\rho}$ itself using two time points. This becomes a question of the trade-off between accuracy and efficiency—a topic beyond the scope of this study.

In principle, the prepared SL magnetization could be read out using any fast imaging sequence, for instance a turbo spin echo sequence (TSE). One possible reason to favor TSE, rather than FLASH, would be its immunity to the potential B_0 field inhomogeneity. However, the potential SAR constraints at 3 T with TSE most likely would slow down its intrinsic speed in clinical applications. Without any concerns on the SAR issues, the employed turbo FLASH sequence in the proposed $R_{1\rho}$ dispersion acquisition has been demonstrated to be nearly as efficient as EPI.[37]

While the implemented SL scheme has been demonstrated to be less prone to the image artefacts associated with non-uniform B_0 and B_1 fields,[32,35] the deviations of actual B_1 fields from the prescribed ones might still have an adverse effect on the accuracy of $R_{1\rho}$ dispersion quantification, particularly on the edged imaging slices in the human knee where the B_1 inhomogeneity (ie ΔB_1) usually deteriorates. In the literature,[47] ΔB_1 has been demonstrated to be relatively small (~5%) in the human knee cartilage, and our previous B_1 mapping (data not shown) was largely consistent with the literature. Nonetheless, it would be of great interest to further investigate to what extent the B_1 mapping could increase the accuracy of $R_{1\rho}$ dispersion quantification in clinical studies.

4.3 | SL-prepared constant M_{prep}

The constant M_{prep} was calculated with the assumed values of R_2^i, R_2^a and τ_b inferred from the literature.[25] It was impossible for the whole cartilage to have a constant M_{prep} across various locations because of an orientation-dependent R_2^a. Nonetheless, if the prepared M_{prep} had been clustered in a narrow range, the expected k-space filtering effect would have been comparable for each segmented acquisition in phase-encoding directions, thus diminishing an adverse T_1 relaxation effect during FLASH imaging readout.[27]

As shown in Figure 5A and 5B, some observed M_{prep} values for different cartilage locations significantly deviated from the designed 60%; however, they were all maintained within a limited dynamic range. It was the variation rather than the absolute value of M_{prep} that had played a key role in imparting the k-space filtering effect on quantifying $R_{1\rho}$. This observation suggests that the precise values of R_2^i, R_2^a and τ_b might not be as essential as initially thought for tailoring a constant M_{prep} in $R_{1\rho}$ dispersion imaging.

As a reference, the prepared M_{prep} using the standard $R_{1\rho}$ dispersion imaging protocol was provided herein, with a range from 98% ($\omega_1/2\pi$ = 1 kHz and T_{SL} = 1 ms) to 23% ($\omega_1/2\pi$ = 125 Hz and T_{SL} = 40 ms) given that $R_2^i = R_2^a = 20$/s, $\tau_b = 300$ μs. It was not surprising then that quantification of $R_{1\rho}$ dispersion became unreliable even without considering the robustness of the SL[7,35] or the possibility of involuntary knee movements when using this lengthy imaging protocol.

4.4 | Quantifying $R_{1\rho}$ dispersion with an REF

The key to the success of $R_{1\rho}$ dispersion quantification depends on integrating additional information derived from the magic angle location in the deep femoral cartilage. This is because the prepared M_{prep} was intended to be constant; in other words, the dynamic range in M_{prep} was limited,

thus leading to unreliable data fitting. Our previous study has documented on how to accurately extract an REF in the deep femoral cartilage,[23] and the defined REF was also applied to the tibial and patellar cartilage in this work, with an assumption of comparable S_0 and R_2^i values across the whole knee cartilage.

Based on the comparison results with the gold standards in Figure 6, it was challenging to positively corroborate this assumption in the current work because of inconsistent results observed in the tibial and patellar cartilage. However, the measured $R_{1\rho}$ and R_2 in the tibial cartilage from both methods were constantly higher than those in the femoral and patellar cartilage, reflective of the fact that the majority of collagen fibers in the tibial cartilage are along B_0. This interesting finding is in accordance with the literature, albeit unspecified.[48]

4.5 | Precision and accuracy of $R_{1\rho}$ dispersion quantification

When excluding some CV_3 for the fitted values (R_2^a, τ_b and S) in the patellar cartilage of the third subject, the precision of $R_{1\rho}$ dispersion measurements seems reasonably good. However, it was still unclear why the repeated scans on the third subject's knee did not produce comparable results only in the patellar cartilage. This observation could not be fully accounted for by an imperfect acquisition protocol. Nonetheless, an informative test of the proposed $R_{1\rho}$ dispersion imaging method was to compare its results with those measured using the state-of-the-art $R_{1\rho}$ mapping sequence (MAPSS).[17]

The observed comparable average $R_{1\rho}$ values in the femoral and tibial cartilage (Figure 6A) lend strong support to the view that the proposed method was not only efficient but also robust in quantifying $R_{1\rho}$ dispersion. It is worth emphasizing that the acquisitions and analyses methods used in the two measurements were fundamentally different, yet the comparable $R_{1\rho}$ values were still attained. The third subject had inconsistent measurement results between two repeated scans in the patellar cartilage, which could be partially responsible for the observed $R_{1\rho}$ deviation from the reference.

Another interesting observation was that the synthetic $R_{1\rho}$ had a larger variation than those based on the MAPSS sequence. It could be the case that the uncertainty of the synthetic $R_{1\rho}$ had been overestimated through multiple-step error propagations. At least one parameter (ie R_2^a) had its variation not completely accounted for with the random Gaussian noise because it was orientation dependent. Further investigations are needed to better understand the observed $R_{1\rho}$ discrepancies with respect to the reported references.

Although comparable values (Figure 6B) were also attained between our fitted R_2 and the references, caution should be exercised when interpreting the comparative results. The R_2 references were actually acquired using a combination of CPMG preparation and MAPSS readout.[49] The reported R_2 from healthy control (n = 7) knee cartilage at 3 T and 7 T were comparable,[43] indicative of hardly any chemical exchange effect contribution to R_2 at 7 T, which is apparently inconsistent with the literature.[50,51] It remains unclear to what extent the previously reported R_2 at 3 T had been compromised by the CPMG-based magnetization preparation, possibly due to a non-trivial spin-locking effect.[52]

4.6 | Limitations

The current work has some limitations. First, no effort was devoted to separating the factors contributing to the improved fitting success rates for the measured $R_{1\rho}$ dispersion profiles. These factors might comprise a fully refocused SL preparation and a limited dynamic range in the SL-prepared magnetizations for turbo-FLASH imaging readout. Second, there was no gold standard for an internal reference used in this study, and thus it became unclear to what extent the reported $R_{1\rho}$ dispersion parameters could have been compromised. Third, the longitudinal magnetization at the end of the FLASH readout was not spoiled, potentially leading to signal inconsistencies among initial SL magnetization preparations. Magnetization reset pulses as employed in MAPSS[17] could be implemented for the developed $R_{1\rho}$ dispersion pulse sequence. Fourth, only a small number of subjects were involved in this study, and data from additional subjects would provide an increased statistical power to support the conclusions. Fifth, analysis of $R_{1\rho}$ dispersion may be unreliable for some locations in the femoral and patellar cartilage, in which the residual dipolar coupling approached zero near the magic angle orientation. Finally, it has been revealed that the contralateral healthy knee may also exhibit molecular changes after ipsilateral knee injury[53]; hence, some changes observed between the repeated scans might be "real" and not attributable to the imaging protocol.

5 | CONCLUSIONS

We have developed a practical $R_{1\rho}$ dispersion imaging protocol for clinical studies of in vivo human knee cartilage at 3 T, which has been demonstrated to be not only efficient but also robust. Although this proposed method was developed for joint cartilage, its underlying principle could be applied to other biological tissues with $R_{1\rho}$ dispersion properties regardless of relaxation mechanisms.

ACKNOWLEDGEMENTS

We would like to thank Professor Thomas Chenevert for support and encouragement, and Suzan Lowe and James O'Connor for help in collecting human knee images. This work was in part supported by the Eunice Kennedy Shriver National Institute of Child Health & Human Development of the National Institutes of Health (NIH) under Award Number 5-R01-HD-093626-02 (to Professor Riann Palmieri-Smith) and a Discovery Grant by the University of Michigan-Peking University Health Science Center (UM-PUHSC) Joint Institute (to Professor Tristan Maerz). The content from this work is solely the responsibility of the authors and does not necessarily represent the official views of the NIH.

DATA AVAILABILITY STATEMENT

Data available on request from the authors.

ORCID

Yuxi Pang https://orcid.org/0000-0001-5039-0236

REFERENCES

1. Vlaardingerbroek MT, Boer JA. *Magnetic Resonance Imaging: Theory and Practice*. Berlin, Heidelberg: Springer Science & Business Media; 2013.
2. Mathur-De Vré R. The NMR studies of water in biological systems. *Prog Biophys Mol Biol*. 1980;35:103-134.
3. Woessner DE. Nuclear magnetic-relaxation and structure in aqueous heterogeneous systems. *Mol Phys*. 1977;34(4):899-920.
4. Peto S, Gillis P, Henri VP. Structure and dynamics of water in tendon from NMR relaxation measurements. *Biophys J*. 1990;57(1):71-84.
5. Knispel RR, Thompson RT, Pintar MM. Dispersion of proton spin-lattice relaxation in tissues. *J Magn Reson*. 1974;14(1):44-51.
6. Duvvuri U, Goldberg AD, Kranz JK, et al. Water magnetic relaxation dispersion in biological systems: the contribution of proton exchange and implications for the noninvasive detection of cartilage degradation. *Proc Natl Acad Sci USA*. 2001;98(22):12479-12484.
7. Pang Y. An order parameter without magic angle effect (OPTIMA) derived from $R_{1\rho}$ dispersion in ordered tissue. *Magn Reson Med*. 2020;83(5):1783-1795.
8. Borthakur A, Mellon E, Niyogi S, Witschey W, Kneeland JB, Reddy R. Sodium and $T_{1\rho}$ MRI for molecular and diagnostic imaging of articular cartilage. *NMR Biomed*. 2006;19(7):781-821.
9. Reddy R, Insko EK, Kaufman JH, Bolinger L, Kneeland JB, Leigh JS. MR imaging of cartilage under spin-locking. In: *Proceedings of the International Society of Magnetic Resonance Medicine, Nice*. 1995:1535.
10. Wang L, Regatte RR. $T_{1\rho}$ MRI of human musculoskeletal system. *J Magn Reson Imaging*. 2015;41(3):586-600.
11. Link TM, Neumann J, Li X. Prestructural cartilage assessment using MRI. *J Magn Reson Imaging*. 2017;45(4):949-965.
12. Link TM, Li X. Establishing compositional MRI of cartilage as a biomarker for clinical practice. *Osteoarthr Cartil*. 2018;26(9):1137-1139.
13. Kim J, Mamoto K, Lartey R, et al. Multi-vendor multi-site $T_{1\rho}$ and T_2 quantification of knee cartilage. *Osteoarthr Cartil*. 2020;28(12):1539-1550.
14. Jones GP. Spin-lattice relaxation in the rotating frame: weak-collision case. *s*. 1966;148(1):332-335.
15. Akella SVS, Regatte RR, Gougoutas AJ, et al. Proteoglycan-induced changes in $T_{1\rho}$-relaxation of articular cartilage at 4T. *Magn Reson Med*. 2001;46(3):419-423.
16. Regatte RR, Akella SVS, Lonner JH, Kneeland JB, Reddy R. $T_{1\rho}$ relaxation mapping in human osteoarthritis (OA) cartilage: comparison of $T_{1\rho}$ with T_2. *J Magn Reson Imaging*. 2006;23(4):547-553.
17. Li X, Han ET, Busse RF, Majumdar S. In vivo $T_{1\rho}$ mapping in cartilage using 3D magnetization-prepared angle-modulated partitioned *k*-space spoiled gradient echo snapshots (3D MAPSS). *Magn Reson Med*. 2008;59(2):298-307.
18. Regatte RR, Akella SV, Borthakur A, Kneeland JB, Reddy R. Proteoglycan depletion-induced changes in transverse relaxation maps of cartilage: comparison of T2 and T1ρ. *Acad Radiol*. 2002;9(12):1388-1394.
19. van Tiel J, Kotek G, Reijman M, et al. Is T1ρ mapping an alternative to delayed gadolinium-enhanced MR imaging of cartilage in the assessment of sulphated glycosaminoglycan content in human osteoarthritic knees? An in vivo validation study. *Radiology*. 2016;279(2):523-531.
20. Shao H, Pauli C, Li S, et al. Magic angle effect plays a major role in both T1rho and T2 relaxation in articular cartilage. *Osteoarthr Cartil*. 2017;25(12):2022-2030.
21. Menezes NM, Gray ML, Hartke JR, Burstein D. T_2 and $T_{1\rho}$ MRI in articular cartilage systems. *Magn Reson Med*. 2004;51(3):503-509.
22. Mlynarik V, Szomolanyi P, Toffanin R, Vittur F, Trattnig S. Transverse relaxation mechanisms in articular cartilage. *J Magn Reson*. 2004;169(2):300-307.
23. Pang Y, Palmieri-Smith RM, Malyarenko DI, Swanson SD, Chenevert TL. A unique anisotropic R2 of collagen degeneration (ARCADE) mapping as an efficient alternative to composite relaxation metric (R2-R1rho) in human knee cartilage study. *Magn Reson Med*. 2019;81(6):3763-3774.
24. Lenk R, Bonzon M, Greppin H. Dynamically oriented biological water as studied by NMR. *Chem Phys Lett*. 1980;76(1):175-177.
25. Wang P, Block J, Gore JC. Chemical exchange in knee cartilage assessed by $R_{1\rho}$ ($1/T_{1\rho}$) dispersion at 3T. *Magn Reson Imaging*. 2015;33(1):38-42.
26. Coremans J, Spanoghe M, Budinsky L, et al. A comparison between different imaging strategies for diffusion measurements with the centric phase-encoded turboFLASH sequence. *J Magn Reson*. 1997;124(2):323-342.
27. Williams CF, Redpath TW. Sources of artifact and systematic error in quantitative snapshot FLASH imaging and methods for their elimination. *Magn Reson Med*. 1999;41(1):63-71.
28. Chen W. Errors in quantitative T1rho imaging and the correction methods. *Quant Imaging Med Surg*. 2015;5(4):583-591.
29. Charagundla SR, Borthakur A, Leigh JS, Reddy R. Artifacts in $T_{1\rho}$-weighted imaging: correction with a self-compensating spin-locking pulse. *J Magn Reson*. 2003;162(1):113-121.
30. Mitrea BG, Krafft AJ, Song RT, Loeffler RB, Hillenbrand CM. Paired self-compensated spin-lock preparation for improved $T_{1\rho}$ quantification. *J Magn Reson*. 2016;268:49-57.
31. Zeng H, Danie LG, Gochberg C, Zhao Y, Avison M, Gore JC. A composite spin-lock pulse for ΔB0 + B1 insensitive T1rho measurement. In: *Proceedings of the 14th Annual Meeting of ISMRM, Seattle, Washington, USA*. 2006:2356.

32. Gram M, Seethaler M, Gensler D, Oberberger J, Jakob PM, Nordbeck P. Balanced spin-lock preparation for B_1-insensitive and B_0-insensitive quantification of the rotating frame relaxation time $T_{1\rho}$. *Magn Reson Med*. 2021;85:2771-2780.
33. Johnson CP, Thedens DR, Kruger SJ, Magnotta VA. Three-dimensional GRE $T_{1\rho}$ mapping of the brain using tailored variable flip-angle scheduling. *Magn Reson Med*. 2020;84(3):1235-1249.
34. Momot KI, Pope JM, Wellard RM. Anisotropy of spin relaxation of water protons in cartilage and tendon. *NMR Biomed*. 2010;23(3):313-324.
35. Pang Y. A self-compensated spin-locking scheme for quantitative R1ρ dispersion in articular cartilage. In: *Proceedings of the 28th Annual Meeting of ISMRM, Paris, France*. 2020:2743.
36. Geerts-Ossevoort, L., De Weerdt, E., Duijndam, A., et al. Compressed SENSE. Speed done right. Every time. *Philips. Compressed SENSE. MR Clinical Application*. 2018. https://philipsproductcontent.blob.core.windows.net/assets/20180109/619119731f2a42c4acd4a863008a46c7.pdf. Accessed September 20, 2019.
37. Norris DG. Excitation angle optimization for snapshot FLASH and a signal comparison with EPI. *J Magn Reson*. 1991. 91(1):190-193.
38. Klein S, Staring M, Murphy K, Viergever MA, Pluim JPW. elastix: a toolbox for intensity-based medical image registration. *IEEE Trans Med Imaging*. 2010;29(1):196-205.
39. Yushkevich PA, Piven J, Hazlett HC, et al. User-guided 3D active contour segmentation of anatomical structures: significantly improved efficiency and reliability. *NeuroImage*. 2006;31(3):1116-1128.
40. Markwardt CB. Non-linear least-squares fitting in IDL with MPFIT. In: Bohlender D, Dowler P, Durand D, eds. *Proceedings of Astronomical Data Analysis Software and Systems XVIII, Quebec, Canada, ASP Conference Series, Vol. 411*. San Francisco, CA: Astronomical Society of the Pacific; 2009:251-254.
41. Bevington PR, Robinson DK. *Data Reduction and Error Analysis for the Physical Sciences*. 3rd ed. Boston, MA: McGraw-Hill; 2003.
42. Motulsky HJ, Ransnas LA. Fitting curves to data using nonlinear regression: a practical and nonmathematical review. *FASEB J*. 1987;1(5):365-374.
43. Wyatt C, Guha A, Venkatachari A, et al. Improved differentiation between knees with cartilage lesions and controls using 7T relaxation time mapping. *J Orthop Transl*. 2015;3(4):197-204.
44. Press WH, Teukolsky SA, Vetterling WT, Flannery BP. *Numerical Recipes in C*. Cambridge, UK: Cambridge University Press; 1988.
45. Sharafi A, Chang G, Regatte RR. Biexponential T_2 relaxation estimation of human knee cartilage in vivo at 3T. *J Magn Reson Imaging*. 2018;47(3):809-819.
46. Mahar R, Batool S, Badar F, Xia Y. Quantitative measurement of T2, T1ρ and T1 relaxation times in articular cartilage and cartilage-bone interface by SE and UTE imaging at microscopic resolution. *J Magn Reson*. 2018;297:76-85.
47. Wang L, Schweitzer ME, Padua A, Regatte RR. Rapid 3D-T_1 mapping of cartilage with variable flip angle and parallel imaging at 3.0T. *J Magn Reson Imaging*. 2008;27(1):154-161.
48. Razmjoo A, Caliva F, Lee J, et al. T_2 analysis of the entire Osteoarthritis Initiative dataset. *J Orthop Res*. 2020;39(1):74-85.
49. Li X, Wyatt C, Rivoire J, et al. Simultaneous acquisition of $T_{1\rho}$ and T_2 quantification in knee cartilage: repeatability and diurnal variation. *J Magn Reson Imaging*. 2014;39(5):1287-1293.
50. Welsch GH, Apprich S, Zbyn S, et al. Biochemical (T2, T2* and magnetisation transfer ratio) MRI of knee cartilage: feasibility at ultra-high field (7T) compared with high field (3T) strength. *Eur Radiol*. 2011;21(6):1136-1143.
51. Jordan CD, Saranathan M, Bangerter NK, Hargreaves BA, Gold GE. Musculoskeletal MRI at 3.0 T and 7.0 T: a comparison of relaxation times and image contrast. *Eur J Radiol*. 2013;82(5):734-739.
52. Santyr GE, Henkelman RM, Bronskill MJ. Variation in measured transverse relaxation in tissue resulting from spin locking with the CPMG sequence. *J Magn Reson*. 1988;79(1):28-44.
53. Ochoa J, Amano K, Tanaka M, et al. Altered biomechanics and cartilage health changes in bilateral knees following unilateral ACL reconstruction: a 2-year follow-up. *Osteoarthr Cartil*. 2016;24:S406-S407.

How to cite this article: Pang Y, Palmieri-Smith RM, Maerz T. An efficient $R_{1\rho}$ dispersion imaging method for human knee cartilage using constant magnetization prepared turbo-FLASH. *NMR in Biomedicine*. 2021;34:e4500. https://doi.org/10.1002/nbm.4500